UJEAS

UNIZIK JOURNAL OF ENGINEERING AND APPLIED SCIENCES

UNIZIK Journal of Engineering and Applied Sciences 3(5), December (2024), 1291 - 1306
Journal homepage: https://journals.unizik.edu.ng/index.php/ujeas

Modelling and Simulation of an Enhanced Finite Element Method for Loss Computation in Power Transformers

Anionovo U. E[1], Nwana C. O[2], Obiora-Okeke C. A.[3], Obute K.C[4], Nworabude E. F[5].
[1,3,4,5]Nnamdi Azikiwe University, Awka, Anambra State.
[2]Federal College of Science and Technology Oko, Anambra State.
[*]Corresponding Author's E-mail: ue.anionovo@unizik.edu.ng

Abstract
The problem of evaluating the various performance characteristics of power transformer such as temperature distribution, flux distribution, and losses, is an age long issue in electrical engineering, and an attempt to manually or analytically evaluate them is very difficult and subject to errors. Hence the development and application of Finite Element Method to complex engineering analysis of this nature. This research presented enhanced finite element model application to Power Transformer loss computation. The method applied is modelling and simulation. The Finite Element Analysis of a 1.25MVA Power Transformer Model was created using the TrafoSolve unit of the Simcenter MAGNET Multi-physics Analysis Software. The input, output voltage, and frequency of operation of the power transformer was defined and inputted into the design parameter section from where the phase current was computed. Other parameters of the Power Transformer were selected as appropriate in the design stage before the mesh generation was carried out by process of double discretization as well as normal adaptive discretization process. The Solution of the Model, covered Finite Element Force Calculation, Thermal Analysis, Short Circuit Analysis, and Harmonic Analysis. In summary, the double discretization result for winding loss 48431.63W, and that of normal adaptive FEM which was 48969.4W, produced a percentage absolute error of 1.11%. For individual coil lose computation, the result showed 1.54% absolute error for the low voltage winding section during the short circuit test, translating to 14320.29W for the double discretization algorithm and 14541.18W for the normal adaptive FEM. This validates the double discretization algorithm developed in this research.

Keywords: Finite Element method, Power transformer, Loss calculation, Double discretization, Finite element analysis

1. Introduction

Finite Element Method (FEM) is a common numerical approach to solutions of differential equations arising in Engineering and mathematical modeling such as the traditional fields of structural analysis, mass transport, heat transfer, fluid flow, and electromagnetic potential. The method of approach in all areas which include model definition (preprocessing), solution and post-processing are the same. Various software solutions had been developed to handle or solve the resulting systems of differential equations that result from the preprocessing stage, likewise the post-processing stage. However, it is vital to note that the accuracy of the resulting solution depends on the accuracy of the model definition which invariably lies on the expertise of the engineer performing the analysis. This includes choice of elements, solution algorithm and parameters of interest required to describe the behavior of the engineering structure to be analyzed. In the solution process, it is required to refine the mesh if the result is not satisfactory. This process from research usually involves change of element type or combination of different element types in the case of complex engineering structure or geometry.

Ana and Bojan (2017), presented the use of a self-developed solver based on Boundary Element Methods (BEM) for electric field calculation of a transformer, based on the approximation of charge density on the transformer winding. They utilized linear functions as the base functions with point-matching method, and integrated the resulting system of equations both analytically and numerically. Additionally, to validate the results obtained, commercial Finite Element Methods (FEM) software was used to model the same problem and the solution obtained for real transformer geometry using both

BEM and FEM. Finally, comparative analyses of the results obtained were presented. The extension of FEM to transformer design and analysis in retrospective was given by (Chitaliya, and Joshi, 2013). They showed the importance of using FEM to determine transformer parameters such as winding impedance, leakage inductance, hot spot temperature etc., during design in a prototype unit.

Leela, Madhumitha, Sindhu, and Maheswari, (2020), emphasized the importance of transformers in the power system domain and therefore suggested the use of FEM in power transformer design. This is because it is easy to analyze the Electromagnetic Field distribution and calculate the losses during design than when implemented in real-time. They went ahead to simulate a three-phase 11/0.4 kV power transformer using the Finite Element Method to demonstrate this idea. Vasantha, and Akthar, (2019), analyzed the impact of conducting particles in the coil of a power transformer using FEM and deduced that part of the stress undergone by power transformers during operation is due to conducting particles in the winding of the transformer. The result suggested design improvement to reduce the effect of electromagnetic stress power transformers could undergo as a result of spurious particles in its winding.

Sweta, and Akshay, (2017) presented 3-D modeling of power transformers for the purpose of predicting the core and winding loses. Test result presented showed a significant improvement in the result obtained using 3-D FEM when compared to experimental results obtained for the same transformer. Vibhuti, and, Deepika (2020), chronicled the application of FEM solution to transformer parameter estimation from 2017 to 2019 revealing a total of 73 publications. These publications, spanned through high voltage and low voltage power transformers as well as three phase transformers. Parameters analyzed by various authors include Copper Loss, Eddy Current Loss, Stray Loss, and short circuit Loss.

To solve the problem associated with dual-weighted residual based adaptivity for time-dependent problems, which is computationally very costly if the spatial and temporal meshes are changed in each time step, Estep et al, (2010), presents a novel method to resolve this issue by using a sequence of fixed but nonuniform spatial meshes in time. The elements of this sequence are called blocks, which is why the method was named block-wise adaptivity. They used goal-oriented posteriori analysis to formulate several strategies on how to select these blocks and still satisfy an overall accuracy in the output function. The strategies were illustrated on different types of evolution Partial Differential Equations (PDEs) in one and three dimensions.

One approach to retain the advantage of such data structures and still have proper and general geometry approximation is to use discontinuous Galerkin method based on Nitsche's method (Johansson, 2010). This idea is not new, but Johansson and Larson, (2010) presented a rigorous procedure to avoid numerical instabilities by associating certain elements on the boundary with elements lying in the interior (Burman and Hansbo, 2009). The method was proved to have optimal convergence and was illustrated on a three-dimensional problem. Erich, Traian and David, (2013), proposed a two-level finite element discretization of the nonlinear stationary quasi-geostrophic equations, which model the wind driven large scale ocean circulation. Optimal error estimates for the two-level finite element discretization were derived and numerical experiments for the two-level algorithm with the Argyris finite element were carried out. The numerical results verified the theoretical error estimates and showed that, for the appropriate scaling between the coarse and fine mesh sizes, the two-level algorithm significantly decreased the computational time of the standard one-level algorithm. The application of these refinement, is seen at work in modern day FEM solution poised to produce more and more accurate results which minimizes design and fabrication loses in electromagnetic devices.

Behnam, Ali, and Fatemeh (2024), in a more recent research work, modelled 1000kVA and 1600kVA power transformer using FEM to ascertain their no-load losses. They further carried out a tripartite comparison of the result with theoretically calculated values and that of experimental result. Their conclusion is that the percentage error for the result obtained using FEM and experimental result were less than 1%, far better than the result obtained using theoretical approach which ranged from 5 – 10% difference. A scan through the base papers presented above showed that the concept of mesh resizing or adaptive mesh reduction during finite element analysis solution is not new, however this concept lacks material base in transformer finite element analysis. Hence, as an addendum to the body of knowledge in this field of engineering analysis, and following these specific objectives which include to study the finite element method and its application to Electrical Engineering problem analysis, ascertain the loss distribution of power transformer using Finite Element Method, model enhanced Finite Element Method using double discretization approach, and implement and simulate the enhanced finite element model in Finite Element environment (TrafoSolve), this article suggests the concept of double discretization or double meshing model to further improve on the accuracy of the model representation at the pre-processing stage. This requires addition of an abstraction layer whose function is to internally split the already generated mesh from the discretization stage, into two creating a kind of neuroadaptive process which would improve the overall results during transformer finite element analysis process.

2. Material and Method

The material used includes TrafoSolve, Simcenter MAGNET, Simcenter MAGNET Thermal simulation software solution, all of version 2212, and personal computer (PC) system used to run the application. The three software are developed by Infologic Design (Infolytica Europe). The PC requirement is at least 20 gigabytes internal storage, 8 gigabyte RAM and 2.4 GHz core i-3 or higher processor. The method employed in this research paper is design, and simulation.

2.1 Double Discretization Algorithm

The concept of double discretization algorithm Integrated to the solver or result unit was created by dividing into half, the various element dimensions of the transformer core, coil, and insulation strips, during mesh formation by means of neuroadaptive process represented in TrafoSolve by dynamic mesh formation. This is a crucial process in pre-processing stage of the Finite Element Analysis.

```
/* Finite Element Discretization Algorithm Verses Double Discretization Algorithm
   (Johansson, 2010)
*/

/* Finite Element Discretization Algorithm */
1: // Choose an initial triangulation Kh and a tolerance TOL.
2: while |m(e)| < TOL do
3: Compute a solution uh to the primal problem.
4: Compute a solution φh to the adjoint problem.
5: Compute an estimate of |m(e)|.
6: ∑|m(e)|
7: if |m(e)| > TOL then
8: LTOL = TOL/|Kh| //Normal discretization step
9: Refine all elements with |m(e)| ≥ LTOL.
10: end if
11: end while
```

Figure 1: Finite Element Discretization Algorithm.

Figure 1 shows a general *h*-adaptive algorithm for handling spatial errors where *h* is global mesh size. *Kh* local mesh size, *TOL* tolerance term, *LTOL* local tolerance term, and $|m(e)|$ mean error term. The process of FE discretization starts by initializing the element mesh size, and the tolerance value which the element must not split below. Then while the mean error value of the element remains less than the tolerance, the algorithm computes the solutions of the meshes generated till the mean error value of the element becomes greater than the tolerance value. At this instance, the algorithms search for convergence which is obtained by mesh refinement given by mean error value greater than or equal to local tolerance.

```
/* Double Discretization Algorithm */
1: // Choose an initial triangulation or element mesh size Kh and a tolerance TOL.
2: initialize kh = a, TOL = b, tn = 0;
3: while |m(e)| < b do
4: Compute a solution uh to the primal problem.
5: Compute a solution φh to the adjoint problem.
6: Compute an estimate of |m(e)|.
7: ∑|m(e)|;
8: if ∑|m(e)| > b then
9: LTOL = TOL/|Kh|;
10: LTOL/2; //Double discretization step
11: Refine all elements with |m(e)| ≥ LTOL.
12: end if
13: end while
```

Figure 2: Double Discretization Algorithm

For the double discretization approach figure 2, the only difference is that the local tolerance value used to refine all elements at convergence period is half the value used in normal FE discretization algorithm. Hence, a finer mesh and a more approximate mean error value is obtained.

The solution process flow depicted in figure 3, involved designing a 1.25MVA transformer using the TrafoSolve unit of the simulation software package by utilizing the transformer model parameters defined in the subsequent sections.

The three-software work together to compute the transformer loses, carryout thermal analysis, and finite element force, and stress analysis of the transformer model designed in this article. In the preceding sections we highlight the various components of the transformer, used for the design.

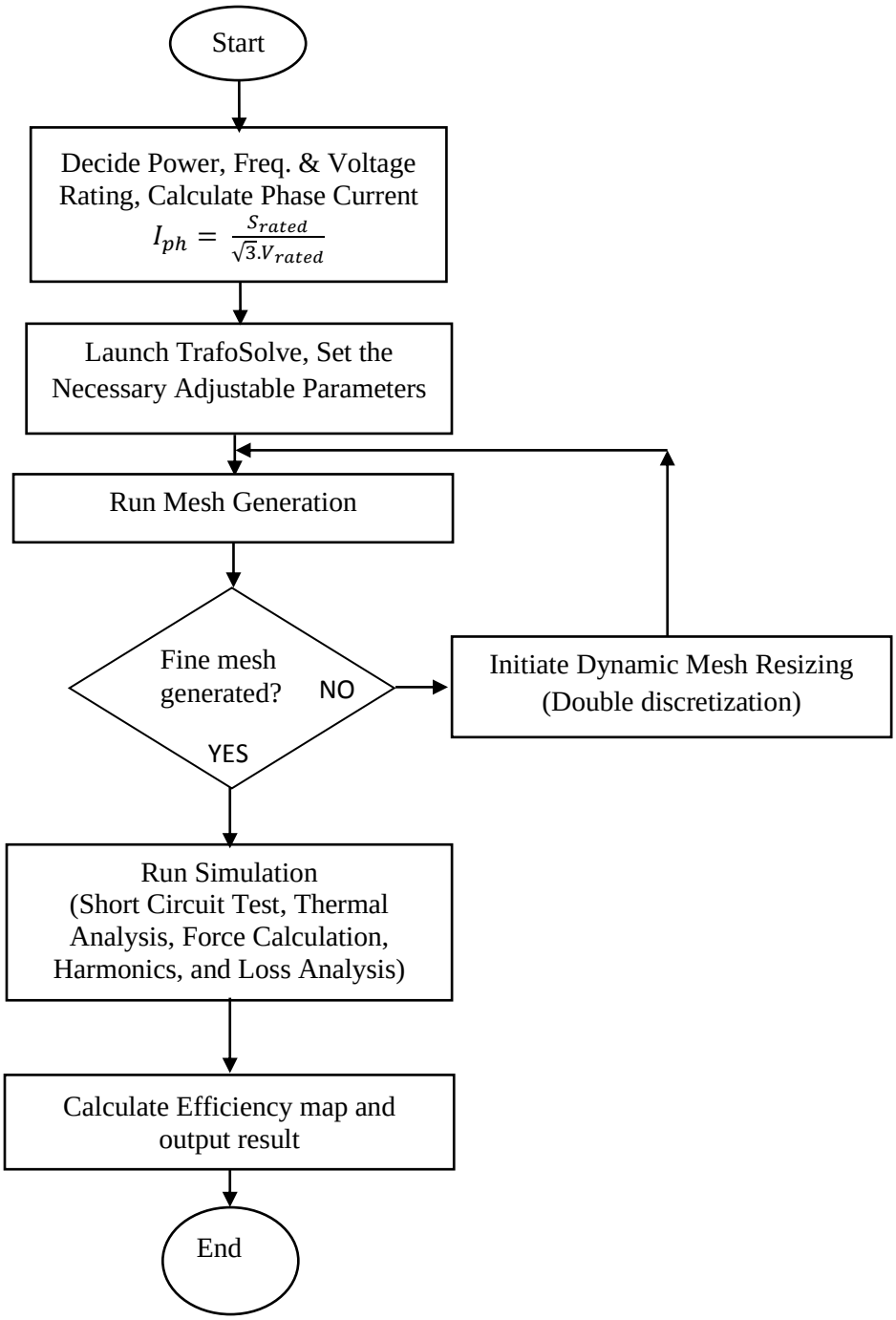

Figure 3: Solution flow chat

2.2 Transformer Loss Model

Iron, copper, dielectric, and miscellaneous losses are the several categories into which transformer losses can be separated. This research work discusses transformer losses in windings and core under harmonic effect. As seen in Equation (1), the overall losses of a transformer can be stated as the sum of the transformer no-load core losses and the load winding losses, in accordance with the IEEE Standard C57.110, and the Steinmetz empirical formula.

$$P_{TL} = \underbrace{(k_1 f B_m^n + k_2 f^2 B_m^2 t^2)\,.\,G + p_F}_{P_{NL}} + \underbrace{P_{I^2R} + P_{EC} + P_{OSL}}_{P_{LL}} \quad (1)$$

where P_{TL} is the transformer's total theoretical loss, which includes P_{NL} and load loss as well as no-load core loss. The current fundamental frequency is P_{LL}. f The silicon core working flux density amplitude is denoted by B_m. t is the thickness of the silicon wafer, and n is the hysteresis coefficient, which is equivalent to 2~2.5. The properties of silicon steel, which can be discovered by experimentation, determine $k_1 and\ k_2$ (Le, 2020). The core mass is denoted by G. The unit core magnetic loss is $k_1 f B_m^n$. The loss of the unit core vortex is $k_2 f^2 B_m^2 t^2$. The core additional loss, or p_F, has a comparatively low proportion. P_{EC} is the additional loss brought on by the neighboring effect and winding skin effect, while P_{OSL} is the transformer winding resistance loss.

2.2.1 Harmonic loss in the transformer core

Equation (2) displays a reduced representation of the transformer unit core loss derived from equation 3.1.

$$P_{NL} = (k_1 f B_m^n + k_2 f^2 B_m^2 t^2) + p'_F \quad (2)$$

where, the core vortex loss coefficient K_c and the core hysteresis loss coefficient K_h, which are solely reliant on the kind of core material, can be used to quantify k_1 and k_2. While p'_F is the transformer unit additional core loss, n is the hysteresis coefficient, which is typically taken to be 2.

Since $B_m = \frac{E_m}{4.44fNA}$ (3)

where E_m is the transformer's induced electromotive potential amplitude, which has a positive correlation with the transformer's primary side voltage. The winding bend is N. The transformer core's effective cross-sectional area is denoted by A. This suggests that the following formula can be used to determine the transformer core loss under single harmonics (Ehsanifar et al, 2021).

$$P_{NL} = \frac{E^2 mh}{4.44^2 N^2 A^2}\left(\frac{K_h}{f} + K_c t^2\right) + p'_F \quad (4)$$

Then to obtain transformer core losses for multiple harmonic cases, equation (4) can be modified as equation (5)

$$P_{NLh} = \frac{1}{4.44^2 N^2 A^2}\sum_{h=2}^{h_{max}} E^2 mh \left(\frac{K_h}{f} + K_c t^2\right) + p'_F \quad (5)$$

Equation (5) states that the transformer core hysteresis loss decreases as the harmonic frequency increases and increases as the primary harmonic voltage content increases. Furthermore, the vortex loss increases in tandem with the primary harmonic voltage concentration. Since the additional losses are so small and have no effect on the trend of no-load losses with frequency, they are treated as constant values in the theoretical calculations reported in this study work.

2.2.2 Harmonic Loss in Transformer Winding

The T-type equivalent model is commonly used to mimic the transformer's working principle while studying the transformer winding harmonic loss. In general, the harmonic winding resistance of the transformer.

$$P_{I^2R} = \sqrt{h} R_{dc} \quad (6)$$

where R_{dc} is the winding DC resistance and h is the harmonic order.

The external power supply can be viewed as the superposition of separate sources of different harmonic components when calculating the transformer loss using the T-type equivalent model, as shown in Figure 4.

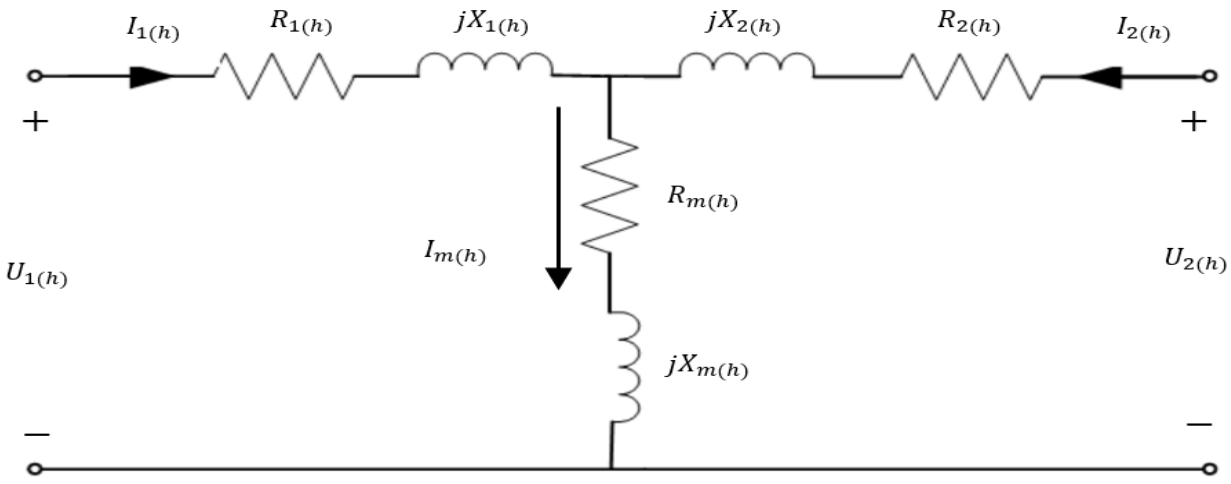

Figure 4: T-type equivalent circuit model of the transformer

In Figure 4, h denotes the harmonic order, while $I_{1(h)}$ represents the major side harmonic current. $I_{2(h)}$ represents the harmonic current on the secondary side of the transformer. $R_{1(h)}$ and $X_{1(h)}$ represent the transformer primary side winding resistance and leakage resistance under the $h-th$ harmonic action. The values $R_{2(h)}$ and $X_{2(h)}$ represent the secondary side winding of the transformer's resistance and reactance under the h-th harmonics. The values $R_{m(h)}$ and $X_{m(h)}$ represent the excitation resistance and impedance of the transformer under the $h-th$ harmonics. When employing the T-transformer equivalent loss model equivalent circuit of a transformer, $R_{(h)}$ is calculated using $\sqrt{h}R_{dc}$ for equivalence. Since the amount of harmonic reactance is proportional to frequency, it is simple to obtain $jX_{(h)} = jhX_{(1)}$. Equation (7) can be used to calculate the active power loss of the transformer's primary side harmonic winding.

$$P_{LLh1} = \sum_{h=2}^{h_{max}} \left| \frac{U_{1(h)} - I_{m(h)}(R_{m(h)} + jX_{m(h)})}{R_{1(h)} + jX_{1(h)}} \right|^2 R_{1(h)} = \sum_{h=2}^{\infty} I^2{}_{1(h)}\, R_{1(h)} \quad (7)$$

The active power loss of the secondary side harmonic winding can also be found using equation (8).

$$P_{LLh2} = \sum_{h=2}^{h_{max}} \left| \frac{\frac{1}{k} I_{m(h)}(R_{m(h)} + jX_{m(h)}) - U_{2(h)}}{R_{2(h)} + jX_{2(h)}} \right|^2 R_{2(h)} = \sum_{h=2}^{\infty} I^2{}_{2(h)}\, R_{2(h)} \quad (8)$$

Note: $k = \frac{N_1}{N_2}$

where N_1 and N_2 represent the transformer's primary and secondary turns, respectively. The ratio of turns is k. Thus, the three-phase transformer's harmonic winding loss calculation relation is as shown in equation (9).

$$P_{Th} = 3(P_{LLh1} + P_{LLh2}) \quad (9)$$

The transformer's excitation reactance increases in response to the harmonic voltage, as shown by equations (7) and (8), producing a comparatively small current value $I_{m(h)}$. $I_{m(h)}\left(R_{m(h)} + jX_{m(h)}\right)$ can therefore be ignored. Harmonic losses in the winding resistance are directly caused by the harmonic current, which also increases winding losses. This leads to a primary connection between the transformer harmonic winding losses and the harmonic current. However, the $\sqrt{h}R_{dc}$ model does not account for the loss P_{OSL} caused by the proximity effect and winding skin effect on the winding resistance. The AC resistance coefficient $1 + \frac{\Psi}{3}\Delta^4$ model was proposed in IEEE Std C57.110™-2018, a revision of IEEE Std C57.110-2008, to accurately characterize the transformer harmonic winding loss (IEEE, 2018).

The harmonic current directly results in harmonic losses in the winding resistance, which in turn increases winding losses. Consequently, the transformer harmonic winding losses and the harmonic current are largely related. Additionally, the $\sqrt{h}R_{dc}$ model does not account for the loss P_{OSL} caused by the proximity effect and winding skin effect on the winding resistance. IEEE Std C57.110™-2018, a revision of IEEE Std C57.110-2008, proposed the AC resistance coefficient $1+\frac{\Psi}{3}\Delta^4$ model as a precise way to characterize the transformer harmonic winding loss (IEEE, 2018).

$$R_{(h)} = (1+\frac{\Psi}{3}\Delta^4)R_{dc} \tag{10}$$

$$\Psi = \frac{5p^2-1}{15} \tag{11}$$

where $R_{(h)}$ is the h-th harmonic winding AC resistance and R_{dc} is the winding DC resistance. The depth of the h-th harmonic winding's skin effect is determined by

$$\Delta = d/\delta_h \tag{12}$$

And

$$\delta_h = \sqrt{2/\omega_h \mu\sigma} \tag{13}$$

The copper wire's electrical conductivity is represented by σ and its magnetic conductivity by μ. The number of winding layers is represented by p. The thickness of each silicon steel sheet is D, and ω_h is the angular frequency of the $h{-}th$ harmonic.

Thus, the three-phase total transformer loss is modified as shown in equation (14).

$$P_{Th} = 3\sum_{h=2}^{h_{max}} \left|\frac{U_{1(h)}}{\left(1+\frac{\Psi}{3}\Delta^4\right)R_{dc}+jhX}\right|^2 (1+\frac{\Psi}{3}\Delta^4)R_{dc} = \sum_{h=2}^{\infty} I^2{}_{1(h)}\,(1+\frac{\Psi}{3}\Delta^4)R_{dc} \tag{14}$$

As an illustration, a real-world 630 kVA transformer is presented by (Qionglin et al, 2013). The transformer has 36 winding layers, a DC resistance of 0.91 Ω, and a thickness of 1.2 mm for the silicon steel sheet. The resistive frequency characteristics of the transformer's harmonic winding model are shown in Figure 5.

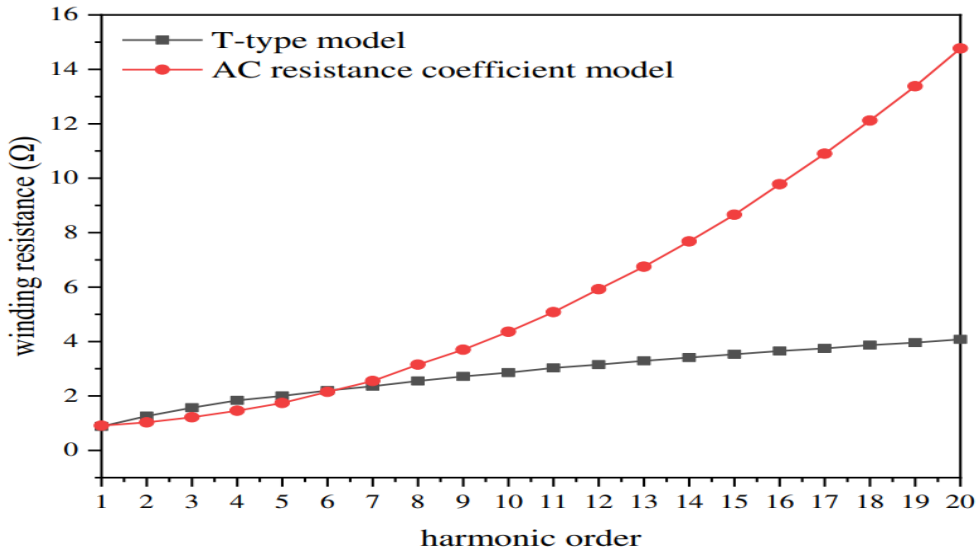

Figure 5: Winding harmonic resistance characteristics of the transformer

When the harmonic frequencies are exceedingly low, the angular frequency values ω_h of the harmonics are also very low. Equations (12) and (13) demonstrate that Δ is incredibly small. Therefore, the value of Δ^4 is negligible. The h-th harmonic winding's AC resistance, R_h, is extremely close to hR_{dc}.

It is evident from harmonic order 2 that the two resistance models currently suit the data well since the skin impact and the proximity effect on the AC resistance are minimal at low frequencies. On the other hand, the value of Δ^4 grows quite dramatically with increasing frequency. $\sqrt{h}R_{dc}$ grows with frequency more slowly. The proximity effect brought in place by the leakage field and the skin effect have an increasing impact on the winding's harmonic resistance, and the two models' descriptions of the winding's harmonic resistance seem to differ significantly in size. Equation (14) makes it clear that there will be a significant discrepancy between the two models when calculating the harmonic current winding losses of the transformer.

2.3 Transformer Field-Circuit Coupling Model

The accuracy of the previously provided transformer model is evaluated by developing a finite element model based on the field-load coupling theory and numerically solving the transformer loss. The Maxwell set of equations below is modified by adding vector magnetic location A and scalar potential $\emptyset$ to produce independent electric field and magnetic field partial differential equations.

$$\begin{cases} B = \nabla \times A \\ E = -\nabla\emptyset \end{cases} \tag{15}$$

The independent partial differential equations for the magnetic and electric fields can be obtained by plugging the equation into the Maxwell equations and is illustrated in equations (16)

$$\begin{cases} \nabla^2 A - \mu\varepsilon\frac{\partial^2 A}{\partial t^2} = -\mu J_s \\ \nabla^2\emptyset - \mu\varepsilon\frac{\partial^2\emptyset}{\partial t^2} = -\frac{\rho}{\varepsilon} \end{cases} \tag{16}$$

The field control equations for the 3D transient field-circuit coupling calculation are shown in matrix form in equation (17). Bojan and Ana (2017).

$$v\nabla \times \nabla \times A + v\nabla.\nabla.A + \sigma\nabla\emptyset + \frac{\partial A}{\partial t}\sigma - J_s = 0 \tag{17}$$

where vector magnetic position is denoted by A. Source current density is denoted by J_s. Reluctivity is denoted by v. Equation (18) can be used to calculate J_s.

$$J_s = \frac{N}{S}i(t).h \tag{18}$$

where N is the winding's number of turns. S is the winding's cross section. Along the coil tangent direction, h is the unit vector.

Figure 6 displays the circuit and electromagnetic field equivalent model coupling computation. The hysteresis loop describes the hysteresis loss produced by the shift of the core magnetic field, while R_e describes the core vortex loss.

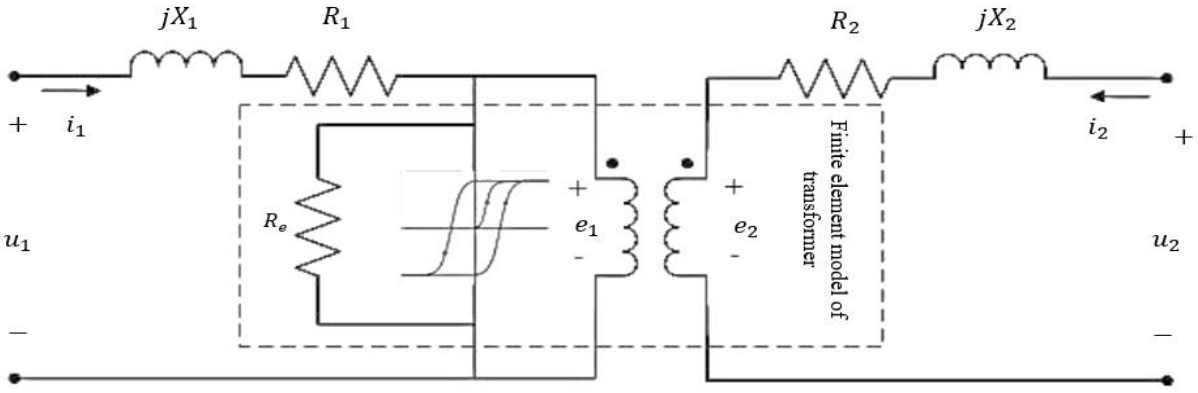

Figure 6Diagram of the field-coupling model's equivalent circuit

The control equation of the circuit is as shown in equations (19) and (20)

$$u = iR + L\frac{di}{dt} + e \tag{19}$$

$$e = \frac{N}{S}\frac{\partial y}{\partial t}\int_{\Omega} Ahd\Omega \tag{20}$$

where the three-phase transformer's core area is represented by Ω. By solving the differential equations (17) through (20), the field-circuit coupling calculation of the three-dimensional model may be realized.
These models all employ direct stiffness method to arrive at the elemental solutions which sums up to give total loses.

2.4 Transformer Model Parameters
The following parameters were chosen for the transformer design created using TrafoSolve and operating parameters calculated.

Table 1: Transformer design parameters

S/No	Parameter	Value
1	Number of phases:	3
2	Rated power, (kVA):	1250
3	Rated Voltage - HV winding, (kV):	6
4	Rated Voltage - LV winding, (kV):	1.2
5	Frequency, (Hz):	50
6	Core type:	3 legs
7	Core material *M4: -silicon -less than 0.5W/kg loss @1.5T:*	*Unisil/alphasil28 M4*
8	Limb diameter, (mm):	300
9	Window height, (mm):	635
10	Limb Pitch, (mm):	575
11	Ambient temperature, (^{0}C):	40
12	Operating temp. of windings (for losses calculation), (^{0}C):	115
13	Lamination factor:	0.955
14	Number of windings:	2

Rated current which is the unknown variable, is obtained from the formula below and the transformer is configured in star-star with the neutral grounded i.e., (Yyn_0) vector group.

$$I_{phHV} = \frac{S_{rated}}{\sqrt{3}.V_{rated}} = \frac{1{,}250{,}000}{\sqrt{3}*6000} = 120.28A \tag{21}$$

$$I_{phLV} = \frac{S_{rated}}{\sqrt{3}.V_{rated}} = \frac{1{,}250{,}000}{\sqrt{3}*1200} = 601.41A \tag{22}$$

The limb and yoke settings were chosen in the general Limb and Yoke settings, Lamination factor of 0.955, Book setting (Steps/Lamination (s) per step of 5/2 were specified. In the Limb Profile tab, Mode is set to Auto, the Limb diameter is set to 300 mm, and tolerance value is set to 0.5 and number of steps set to 8 and the model saved.
Winding material wire schematic is shown in figure 7 below.

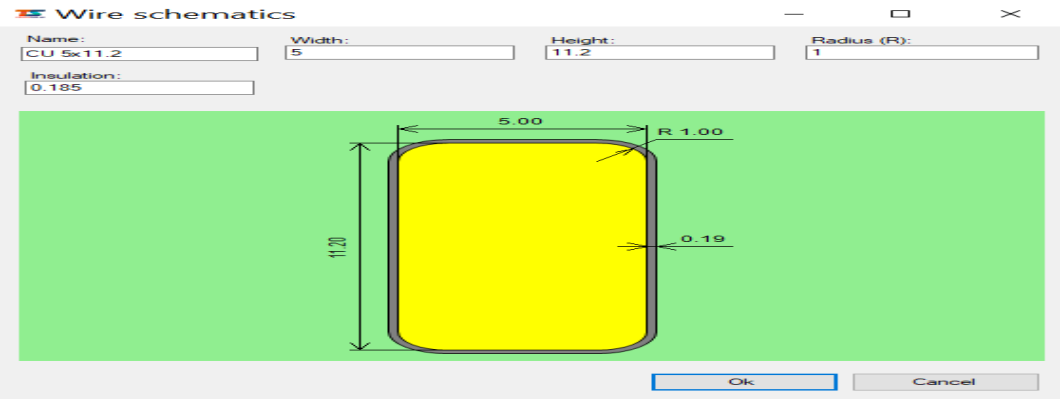

Figure 7: Wire Schematics

Table 2 shows adjustable parameters of wires which when applied calculates other parameters. For the winding circuit section, all winding connections are in series for both high voltage and low voltage section. The source type is set to Current Driven for the High voltage end and Short Circuit for the Low voltage end of the coils.

Table 2: Adjustable wire parameters

Name	Inner Diameter, (mm)	Outer Diameter, (mm)	Height, (mm)	Position, (mm)	# of turns	# of active turns	Coil Type	Strands in hard
HV_1	478	488.74	520.65	577.825	45	45	Stranded	1
HV_2	489.94	500.68	520.65	577.825	45	45	Stranded	1
HV_3	521.88	532.62	520.65	577.825	45	45	Stranded	1
HV_4	533.82	544.56	404.95	519.975	35	35	Stranded	1
LV_1	343.00	419.00	563.8	599.40	34	34	Stranded	29

In the Coil Cast section of the transformer model, the cast setting is applied to every coil for the High voltage end and to Windings for the low voltage end, whereas material type is set to Epoxy. The Radial and Axial thickness is set to 0.1 mm both for the High and Low voltage end.

The current distribution on the power transformer coils is obtained using equation (21) and (22). The component $U_{1(h)}$ represents the applied voltage vector, which in this case is 6kV for high voltage winding section and 1.2kV for low voltage winding section. The parameter $R_{1(h)}, R_{2(h)}, and\ R_{m(h)}$ are representing resistances of varies element of the transformer coil.

The effective forces exerted on each element of the transformer caused by the applied potential difference is obtained using equation (23), in which the parameter $\boldsymbol{U}$ is the effective displacement of all the elements put together, the parameter $\boldsymbol{R}$ represents the reaction force exacted on the transformer element during its operation.

$$\boldsymbol{KU = R} \tag{23}$$

Finally, the parameter $\boldsymbol{K}$ is a constant of proportionality representing the element's stiffness matrices. Equation (24) is the summation of the structure stiffness matrices of the transformer, obtained by direct summation which is referred to as the ***direct stiffness method***.

$$\boldsymbol{K} = \sum_{\boldsymbol{i=1}}^{\boldsymbol{5}} \boldsymbol{K^{(i)}} \tag{24}$$

Losses inherent in the power transformer, such as I^2R losses or Ohmic losses as well as stray losses, short circuit losses, and eddy current loses were computed elementarily and summed up to obtain the transformer total losses.

3. Result

In the result node of TrafoSolve, several calculations were performed using the previously set parameters in chapter three. But before starting the simulation, the following parameters was activated and adjusted accordingly. MagNet Visible - Checked, Close after Solve – unchecked, Accuracy set to Fast (1), Coupling settings, is short circuit test only and the model mesh settings is 11.050 mm.

Since TrafoSolve is coupled to Simcenter MAGNET, the MAGNET interface is evoked when the solution process begins. The 3D model of the power transformer is shown here with the active solution techniques which include the adaptation method or neuro-adaptive process, Newton's method and the Code Generation method.

3.1 Simulation Results

The transformer short circuit analysis, force calculation, thermal analysis and harmonic analysis was performed and the results presented as follows.

Table 3: Short Circuit Analysis; Total Losses

Reactance, XL_{cc}(%)	**Resistance R_{cc} (%)**	**Capacitance XC_{cc} (%)**
6.4	3.875	5.094
Winding loses total (W)	**Winding loses Ohmic (W)**	**Winding loses Eddy (W)**
48431.63	48121.06	310.571



Figure 8: Short circuit Winding loses

As indicated in figure 8, the bulk of the winding loses in contributed by the ohmic or I^2R lose with eddy lose caused by circulating eddy current being very small as expected.

Table 3 shows the percentage Reactance, Resistance and Capacitance of the transformer core and coil. The total winding losses, Ohmic and Eddy are also depicted on this table.

Table 4: Short Circuit Analysis; Winding Losses

S/no	Winding	Current, (A)	Phase, (deg°)	Ohmic Losses, (W)	Circulating Losses, (W)	Eddy Axial, (W)	Eddy Radial, (W)	Eddy Total, (W)	Total Losses, (W)	Eddy / Ohmic	DC Resistance, (mOhm)	Total Mass, (kg)
1	HV	120.281	-90	5165.573	0	245.01	60.163	305.173	5470.745	0.059	119.015	402.531
2	LV1	601.394	90.001	42955.49	-----	4.249	1.148	5.398	42960.88	0	39.589	27.053

Table 4, illustrate the individual winding losses, that is the high voltage winding and the low voltage winding, indicating different types of winding losses as well as the total copper mass of the windings.

Table 5: Short Circuit Analysis; Coil Losses

S/no	Coil	Current, (A)	Phase, (deg°)	Ohmic Losses, (W)	Circulating Losses, (W)	Eddy Axial, (W)	Eddy Radial, (W)	Eddy Total, (W)	Total Losses, (W)	Eddy /Ohmic	Cross Section, (mm2)	Current Density, (A/mm2)	DC Resistance, (mOhm)	Mass, (kg)
1	HV_1	120.281	-90	432.293	0	49.638	4.997	54.635	486.928	0.126	55.142	2.181	29.88	33.687
2	HV_2	120.281	-90	442.972	0	23.587	5.741	29.329	472.3	0.066	55.142	2.181	30.618	34.519
3	HV_3	120.281	-90	471.537	0	7.815	6.712	14.527	486.064	0.031	55.142	2.181	32.593	36.745
4	HV_4	120.281	-90	375.056	0	0.63	2.603	3.233	378.289	0.009	55.142	2.181	25.924	29.226
5	LV1_1	601.394	90.001	14318.5	0	1.416	0.383	1.799	14320.29	0	24.785	24.264	39.589	9.018

Table 5 shows the loss distribution of the individual coils, connected in series to form the winding of the transformer.

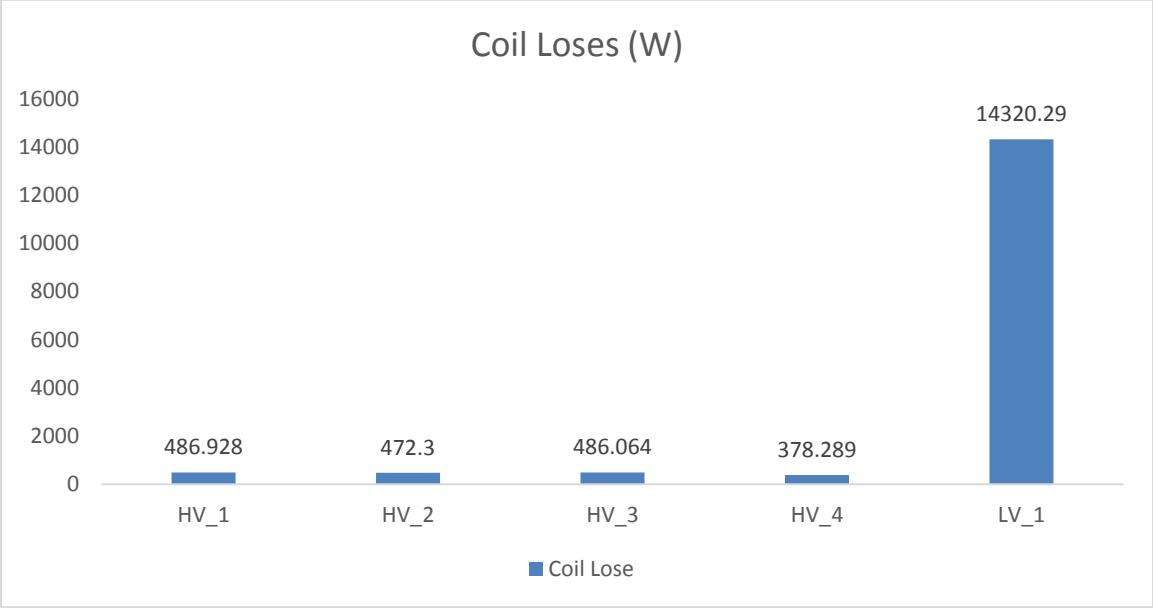

Figure 9: Short circuit Coil loses

Figure 9 plotted from table 5, using the values in the total loss column indicates that bulk of the loses occur in the low voltage coil section. This is expected because the load was connected at this section of the transformer, and during short circuit test, it was the low voltage section that was short circuited.

Table 6: Short circuit Winding lose comparison

Winding loses (W)	Double Discretized FEMA	Normal FEMA	% Absolute error
Ohmic	48121.06	48651.12	1.10
Eddy	310.571	315.28	1.52
Total	48431.63	48969.4	1.11

As modelled in section 2.1, the simulation of the transformer model was in two phases; the Normal Finite Element Algorithm (N-FEMA), and the Double Discretization Finite Element Algorithm (DD-FEMA). Table 6 compares the total winding loses obtained during the simulation with the percentage absolute error computed. The error percentages indicate a strong correlation between the developed model and the already existing FEM adaptive model. However, it is obvious that the double discretization model produced smaller loses which can be attributed to the finer mesh introduced by this approach, thus validating the goal of this model. This process reduced the approximation error to the barest minimum.

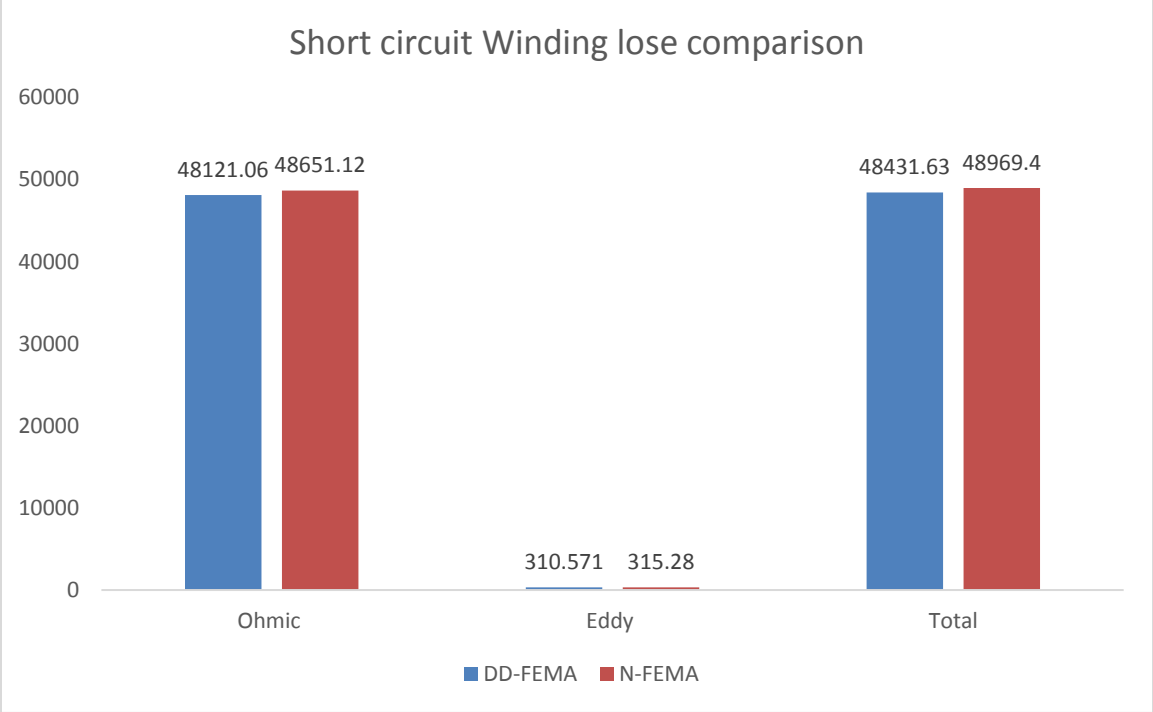

Figure 10: Short circuit Winding lose comparison

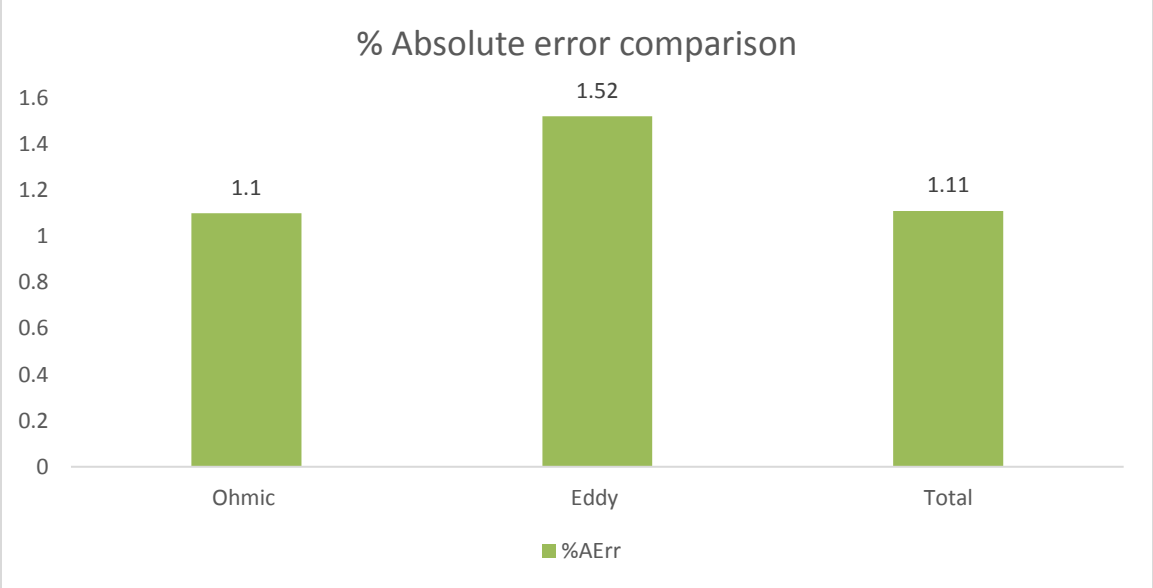

Figure 11: Short circuit Winding lose absolute error comparison

Figure 10, depicts a column chart representation of the model winding loss comparison, which briefly showed that the difference in the result obtained from each model is very small. Figure 11, showed the percentage error comparison, and here the total error of 1.1% clearly indicate that the error difference is very small as well, thus further validating the precision of the developed model or algorithm.

Table 8: Short circuit Total coil lose comparison

Coil	D-DFEMA(W)	N-FEMDA(W)	% Absolute error
HV_1	486.928	491.818	1.00
HV_2	472.3	480.2	1.67
HV_3	486.064	494.011	1.63
HV_4	378.289	382.12	1.01
LV1_1	14320.29	14541.18	1.54

Table 8 shows the individual coil lose comparison during short circuit test, as well as the absolute percentage error associated with the computation. In each case the difference is between 1.0% and 2.0% which is an acceptable value as it indicates that the difference in the model output is very small.

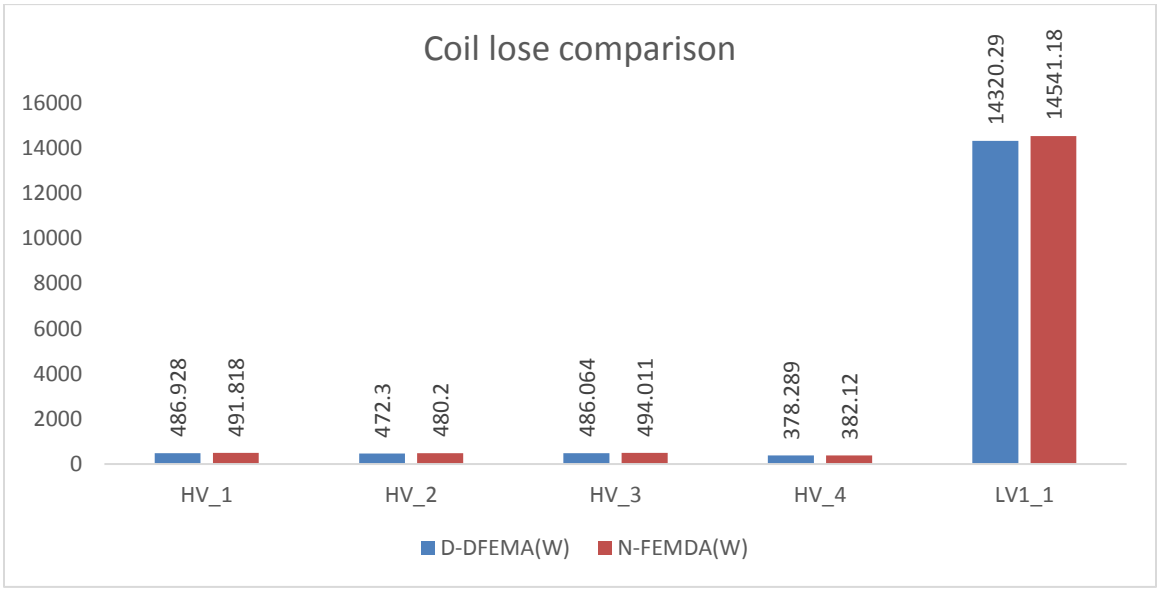

Figure 12: Short circuit coil lose comparison

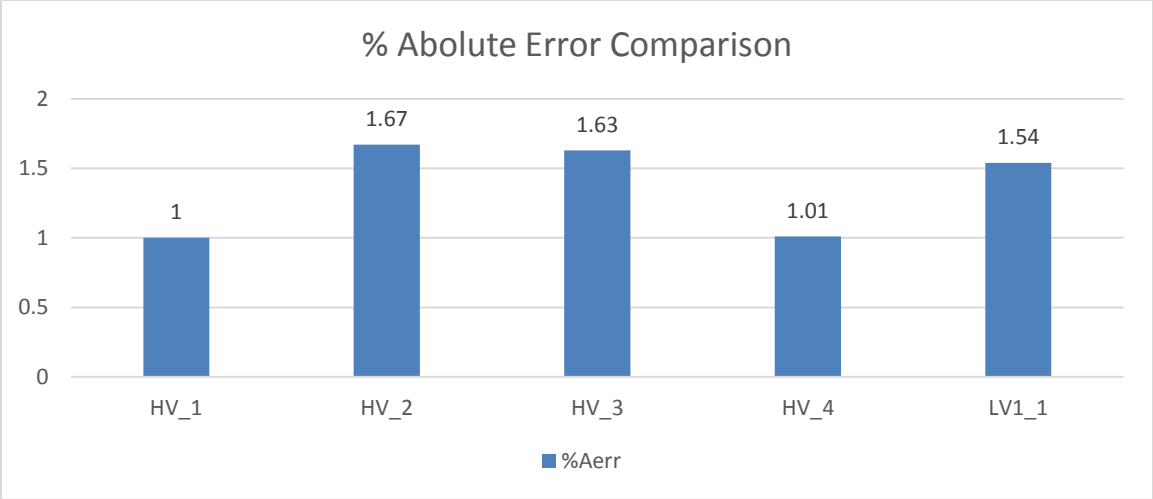

Figure 13: % Absolute coil lose error comparison

Figure 12, shows a column chart representation of the model individual coil loss comparison, which fleetingly showed that the difference in the result obtained from each model is very small. Figure 13, presented the percentage error comparison, and here the difference which is between 1.0% and 2.0% is an acceptable value as it indicates that the difference in the model output is very small. This further validated the accuracy of the developed algorithm.

4. Conclusion

Finite element analysis method as applied to power transformer loss computation had been examined in this research. During the research, it was noted that reasonable number of research data are available in this domain, though most of them are based on adaptive FEM and standard coarse mesh FEM. In this research the application of adaptive finite element analysis method, which is a Multiphysics scenario was examined. And double discretization algorithm or model developed in this research was applied to simulate the winding and the coil loss of the same transformer, finer mesh was obtained and hence better results. In summary, the double discretization result for winding loss 48431.63W, and that of normal adaptive FEM is 48969.4W, produced a percentage absolute error of 1.11%. For individual coil loss computation, the result showed 1.54% absolute error for the low voltage winding section during the short circuit test, translating to 14320.29W for the double discretization algorithm and 14541.18W for the normal adaptive FEM. This validates the double discretization algorithm developed in this research.

5. Recommendation

The use of finite element analysis method in transformer loss calculation is highly recommended owing to its accuracy and the tendency of the method to help manufacturers mitigate design errors.

6. References

Ana Drandića and Bojan Trkulja (2017), *"Transformer electric field calculation using BEM and FEM"* 4th International Colloquium "Transformer Research and Asset Management, Procedia Engineering 202, pgs. 312–318.

Behnam Hashemi, Ali Asghar Taheri, and Fatemeh Jozi (2024), *"Analysis of Transformer No-Load Loss Using Finite Element Method Validated by Experimental Tests"*. Research Square, 4(4), https://doi.org/10.21203/rs.3.rs-4296132/v1

Burman, E. and Hansbo, P. (2009), "*An Interior-penalty-stabilized Lagrange multiplier method for the finite-element solution of elliptic interface problems"*, IMA J Numer Anal.

Chitaliya G. H. and Joshi S. K. (2013), *"Finite Element Method for Designing and Analysis of the Transformer – A Retrospective"* Proc. of Int. Conf. on Recent Trends in Power, Control and Instrumentation Engineering, Association of Computer Electronics and Electrical Engineers. DOI: 03. LSCS.2013.7.524

Ehsanifar, A.; Allahbakhshi, M.; Tajdinian, M.; Dehghani, M.; Montazeri, Z.; Malik, O.; Guerrero, J.M. (2021**),** *"Transformer inter-turn winding fault detection based on no-load active power loss and reactive power."* Int. J. Electr. Power Energy Syst., 130, 107034. [CrossRef]

Erich L. Foster; Traian Iliescu; and, David R. Wells (2013), *"A two-level finite element discretization of the stream function formulation of the stationary quasi-geostrophic equations of the ocean"* Computers and Mathematics with Applications, ScienceDirect, Elsevier Ltd. All rights reserved.

Estep, D.; Carey, V.; Johansson, A.; Larson, M. and, Tavener, S. (2010), "*Blockwise Adaptivity for Time Dependent Problems Based on Coarse Scale Adjoint Solutions"*, accepted to SIAM Journal on Scientific Computing.

Johansson A. (2010), *"Duality-Based Adaptive Finite Element Methods with Application to Time-Dependent Problems*" Doctoral Thesis No. 45, Department of Mathematics and Mathematical Statistics Umea University.

Johansson, A. and, Larson, M. (2010), "*A Discontinuous Galerkin Nitsche Method for Elliptic Problems on Fictitious Domains*, preprint".

Leela Nivashini M.; Madhumitha K.; Sindhu S.; and Maheswari R. V. (2020), "*Design Of High Voltage Transformer Using Finite Element Method"*, International Journal Of Scientific & Technology Research Volume 9, Issue 03.

Qionglin, L.; Lei, Z.; Huijin, L.; Xue, C.; Zhenan, Z.; Shangbei, F. (2013)**, "***Simulation calculation and experimental research on harmonic loss of power transformers."* Power Grid Technol, 37, 3521–3527. [CrossRef]

Sweta A Jain and Dr. Akshay A Pandya (2017), *"Three Phase Power Transformer Modeling Using FEM for Accurate Prediction of Core and Winding Loss"* Kalpa Publications in Engineering, Volume 1, 2017, Pages 75-80.

Vasantha Gowri N. and Zainab Akthar (2019), *"Finite Element Analysis of Power Transformer",* International Journal of Mechanical Engineering and Technology10(3), pp. 1384–1391. [CrossRef]

Vibhuti, Genius Walia and Deepika Bhalla (2020), *"Assessment of the use of FEM for computation of Electromagnetic Forces, Losses and Design of Transformers"* International Conference on Future of Engineering Systems and Technologies Journal of Physics: Conference Series 1478 012029, IOP Publishing doi:10.1088/1742-6596/1478/1/012029.